Investigating the non-idealities in adsorption of CO2-bearing mixtures in cation-exchanged zeolites

Krishna, R.; van Baten, J.M.

DOI
10.1016/j.seppur.2018.06.009

Publication date
2018

Document Version
Final published version

Published in
Separation and Purification Technology

Separation and Purification Technology 206 (2018) 208–217

Contents lists available at ScienceDirect

Separation and Purification Technology

journal homepage: www.elsevier.com/locate/seppur

Investigating the non-idealities in adsorption of CO_2-bearing mixtures in cation-exchanged zeolites

Rajamani Krishna[a,*], Jasper M. van Baten[b]

[a] Van 't Hoff Institute for Molecular Sciences, University of Amsterdam, Science Park 904, Amsterdam 1098 XH, The Netherlands
[b] AmsterCHEM, Almería, Spain

ARTICLE INFO

Keywords:
CO_2 capture
Extra-framework cations
Inhomogeneous distribution
Congregation effects
Real adsorbed solution theory

ABSTRACT

Cation-exchanged zeolites have significant potential for capture of CO_2 from a wide variety of mixtures containing N_2, H_2, alkanes and alkenes. The strong coulombic interactions of CO_2 with extra-framework cations result in strong binding and selective capture. Published experimental data on mixture adsorption indicate that the Ideal Adsorbed Solution Theory (IAST) fails to provide accurate estimates of mixture adsorption equilibrium. The reasons for the quantitative failure of IAST estimates are investigated with the aid of Configurational-Bias Monte Carlo (CBMC) simulations of mixture adsorption. Computational snapshots indicate that the failure of the IAST is traceable to inhomogeneous distribution of adsorbates within the zeolite framework.

1. Introduction

Cation-exchanged zeolites are potent adsorbents for selective capture of CO_2 in natural gas purification, flue gas cleaning, and hydrogen purification processes [1–16]. Coulombic interactions of CO_2 with the extra-framework cations result in strong binding; the binding strength and selectivity can be tuned by appropriate choice of the extra-framework cations, and adjustment of the Si/Al ratios [3,13,17], For the design and development of CO_2-capture technologies, that are normally conducted in fixed-bed adsorbers [18–20], the Ideal Adsorbed Solution Theory (IAST) of Myers and Prausnitz [21] is widely used for calculation of mixture adsorption equilibrium [2,8,15,17,22–26].

Briefly, in the IAST, the partial fugacities in the bulk fluid mixture are related to the mole fraction in the adsorbed phase $x_i = \frac{q_i}{q_1+q_2}$ by the analogue of Raoult's law for vapor-liquid equilibrium, i.e. $f_i = P_i^0 x_i$; $i = 1, 2$ where P_i^0 is the pressure for sorption of every component i, which yields the same spreading pressure, π for each of the pure components, as that for the mixture:

$$\frac{\pi A}{RT} = \int_0^{P_1^0} \frac{q_1^0(f)}{f} df = \int_0^{P_2^0} \frac{q_2^0(f)}{f} df \quad (1)$$

The units of $\frac{\pi A}{RT}$, also called the adsorption potential [23,27–29], are mol kg^{-1}. If the *pure* component adsorption $q_i^0(f)$ isotherm are described by, say, the dual-site Langmuir-Freundlich isotherm $q^0(f) = q_{A,sat}\frac{b_A f^{\nu A}}{1+b_A f^{\nu A}} + q_{B,sat}\frac{b_B f^{\nu B}}{1+b_B f^{\nu B}}$, each of the integrals in Eq. (1) can be evaluated analytically. For specified partial fugacities in the bulk fluid phase, f_i, these constraints may be solved simultaneously, to yield the set of values of the adsorbed phase mole fractions, x_i, and P_i^0, all of which must satisfy Eq. (1). The corresponding values of the integrals using these values of P_i^0 as upper limits of integration must yield the same value of $\frac{\pi A}{RT}$ for each component.

A number of experimental data on mixture adsorption equilibrium reveal the IAST does not provide accurate estimates of component loadings, and adsorption selectivities, especially for operations at high guest occupancies [27,29]. As illustration, Fig. 1a,b,c present comparisons of experimental data on adsorption selectivity with IAST estimates for CO_2/CH_4 and CO_2/N_2 mixtures in NaX (trade name = 13X) and LTA-5A zeolites. The IAST selectivity estimates are about an order of magnitude higher than those determined experimentally. The experimental data for selectivity of adsorption of CO_2/C_3H_8 mixtures in 13X, ZSM-5 (Si/Al = 15), and H-MOR zeolites show that the selectivity decreases with increased mole fraction of CO_2 in the bulk gas mixture, $y_1 = \frac{f_1}{f_1+f_2}$. On the other hand, the IAST predicts the selectivity to increase, albeit slightly, with the mole fraction of CO_2 in the bulk gas

* Corresponding author.
E-mail address: r.krishna@contact.uva.nl (R. Krishna).

https://doi.org/10.1016/j.seppur.2018.06.009
Received 24 April 2018; Received in revised form 22 May 2018; Accepted 2 June 2018
Available online 02 June 2018
1383-5866/

Nomenclature

A	surface area per kg of framework, $m^2\ kg^{-1}$
b_i	Langmuir-Freundlich parameter,$Pa^{-\nu}$
C	constant used in Eq. (3), $kg\ mol^{-1}$
f_i	partial fugacity of species i, Pa
f_t	total fugacity of bulk fluid mixture, Pa
p_i	partial pressure of species i, Pa
p_t	total system pressure, Pa
P_i^0	sorption pressure, Pa
q_i	molar loading species of species i, $mol\ kg^{-1}$
$q_{i,sat}$	molar loading of species i at saturation, $mol\ kg^{-1}$
q_t	total molar loading of mixture, $mol\ kg^{-1}$
Q_i	volumetric uptake of species i, $Q_i = \rho q_i$, $mol\ m^{-3}$
ΔQ	separation potential, $mol\ m^{-3}$
R	gas constant, $8.314\ J\ mol^{-1}\ K^{-1}$
S_{ads}	adsorption selectivity, dimensionless
T	absolute temperature, K
x_i	mole fraction of species i in adsorbed phase, dimensionless
y_i	mole fraction of species i in bulk fluid mixture, dimensionless

Greek letters

γ_i	activity coefficient of component i in adsorbed phase, dimensionless
Λ_{ij}	Wilson parameters, dimensionless
ν	Freundlich exponent in unary isotherm, dimensionless
π	spreading pressure, $N\ m^{-1}$
ρ	framework density, $kg\ m^{-3}$

Subscripts

1	referring to species 1
2	referring to species 2
i,j	components in mixture
i	referring to component i
t	referring to total mixture
sat	referring to saturation conditions

Superscripts

0	referring to pure component loading

mixture; see Fig. 1 d,e,f. There are several other examples of failures of the IAST estimations for mixture adsorption in a variety of cation-exchanged zeolites [4,30,31].

The primary objective of this communication is to gain some insights into the reasons for the failure of the IAST to match the experimental data, as witnessed in Fig. 1. Towards this end, Configurational-Bias Monte Carlo (CBMC) simulations on unary isotherms and mixture adsorption equilibrium were performed using the simulation methodology that is firmly established in the literature [6,7,32–34]. The force field information are taken from García-Sanchez et al.[35], and Dubbeldam et al.[36].

The Supplementary Material accompanying this publication provides (a) details of experimental data and CBMC simulation data for mixture adsorption, (b) unary isotherm fits for all the guest/host combinations examined in this article, (c) details of the IAST, and Real Adsorbed Solution Theory (RAST) methodologies and calculations for mixture adsorption equilibrium, and (d) Wilson parameter fits for thermodynamic non-idealities.

2. CBMC simulations of mixture adsorption in cation-exchanged FAU zeolites

We first investigate $CO_2(1)/C_3H_8(2)$ mixture adsorption in NaX zeolite, that has the Faujasite (FAU) topology consisting of cages of 786 $Å^3$ volume, separated by 7.3 Å 12-ring windows. Each unit cell of NaX zeolite has 106 Si, 86 Al, 86 Na^+ with Si/Al = 1.23. Two different CBMC simulation campaigns were conducted:

(i) The mole fraction of $CO_2(1)$ in the bulk gas phase is held constant, $y_1 = 0.5$, and the bulk gas phase fugacity $f_t = f_1 + f_2$ was varied, and
(ii) The mole fraction of $CO_2(1)$ in the bulk gas phase, y_1 was varied from 0 to 1, keeping the bulk gas phase mixture fugacity $f_t = f_1 + f_2$ constant at a value of 1 MPa.

The results of these two separate campaigns are presented in Fig. 2. In the Henry regime of adsorption, prevailing at $f_t < 10$ kPa, the component loadings of CO_2, and C_3H_8 are nearly equal to each other (cf. Fig. 2a), and the $CO_2(1)/C_3H_8(2)$ adsorption selectivity, S_{ads}, is close to unity (cf. Fig. 2b). With increasing values of the bulk gas phase fugacity f_t, above about 100 kPa, the adsorption becomes increasingly in favor of CO_2, due to strong Coulombic interactions with the extra-framework Na^+ cations. The IAST estimates for the adsorption selectivity are plotted as dashed lines in Fig. 2b. At $f_t = 1$ MPa, the value of $S_{ads} \approx 4$; the IAST estimate is a factor two higher than those determined from CBMC simulations.

The CBMC simulations for $f_t = 1$ MPa, and varying mole fractions of $CO_2(1)$ in the bulk gas phase, y_1, are shown in Fig. 2c. The CBMC simulations show that the adsorption selectivity decreases with increasing proportion of $CO_2(1)$ in the bulk gas phase; see Fig. 2d. On the other hand, the IAST anticipates S_{ads} to increase with increasing y_1. This trend is the same as that witnessed for the experimental data for $CO_2(1)/C_3H_8(2)$ mixture adsorption in NaX zeolite; see Fig. 1d.

The failure of the IAST to provide quantitatively accurate estimates of component loadings, and adsorption selectivities is attributable to the inhomogeneous distribution of adsorbates in the pore space of NaX zeolite, caused by strong binding of CO_2 with the extra-framework cations. The inhomogeneous distribution is clearly visualized in the computational snapshot in Fig. 3 for $f_1 = 0.45$ MPa, and $f_2 = 0.55$ MPa. We note that the top left cage contains only CO_2, and there is no C_3H_8 present in that cage. One of the key assumptions of the IAST is that the distribution of adsorbates within the pore space is homogenous; this assumption is violated causing the quantitative failure of the IAST.

Since the root cause of the failure of the IAST is the inhomogeneous distribution of adsorbates engendered by strong binding of CO_2 with the extra-framework cations, we should expect the non-ideality effects to be negligibly small in all-silica zeolites, with no extra-framework cations. In order to verify this, we performed CBMC simulations $CO_2(1)/C_3H_8(2)$ mixture adsorption in all-silica FAU zeolite, with Si/Al → ∞, at 300 K and total fugacity $f_t = 1$ MPa, with varying CO_2 in the

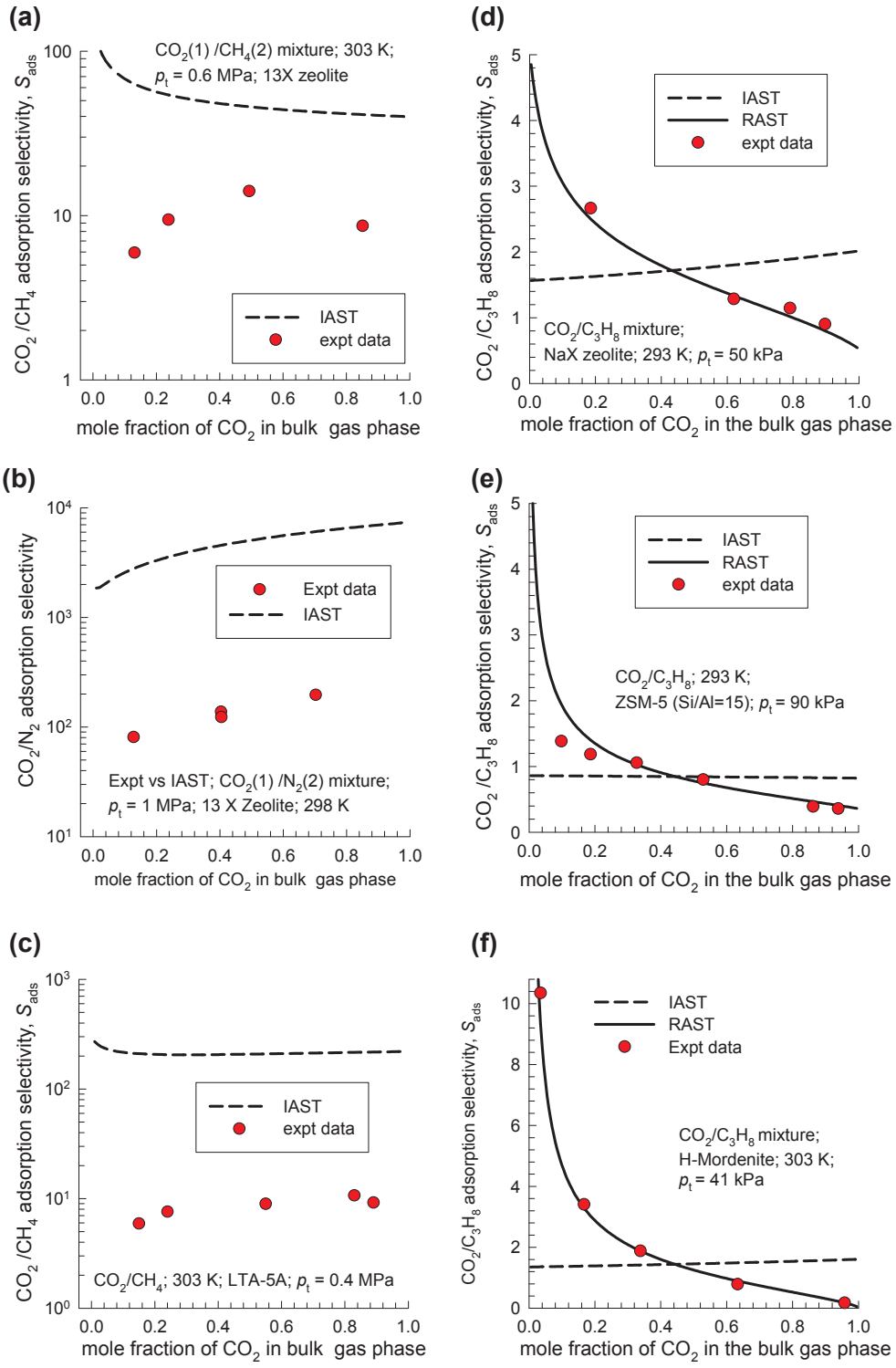

Fig. 1. Comparison of experimental data on mixture adsorption selectivity with IAST estimates for (a) CO_2/CH_4 in 13X zeolite at $T = 298$ K and $p_t = 1$ MPa [10], (b) CO_2/N_2 in 13X zeolite at $T = 298$ K and $p_t = 1$ MPa [11], (c) CO_2/CH_4 in LTA-5A zeolite at $T = 303$ K and $p_t = 0.4$ MPa [12], (d) CO_2/C_3H_8 in 13X zeolite at $T = 293$ K and $p_t = 50$ kPa [40], (e) CO_2/C_3H_8 in ZSM-5 (Si/Al = 15) at $T = 293$ K and $p_t = 90$ kPa [41], and (f) CO_2/C_3H_8 in H-MOR (= H-Mordenite) at $T = 303$ K and $p_t = 41$ kPa and [29]. In all cases, the x-axis represents the mole fraction of CO_2 in the bulk gas phase, maintained at constant total pressure, p_t, and temperature, T. All data inputs and computational details are provided in the Supplementary Material.

bulk gas phase; the results are presented in Fig. 4a. As anticipated, the IAST estimates of component loadings, and adsorption selectivities are in good agreement with CBMC data. Similar good agreement is also obtained for $CO_2(1)/C_2H_6(2)$ mixture adsorption in all-silica FAU zeolite; see Fig. 4b.

From the data in Figs. 2 and 4, we must conclude that the accuracy of IAST estimates should also depend on the Si/Al ratio of cation-exchanged zeolites. To test this hypothesis Fig. 5 presents a comparison of CO_2/CH_4 adsorption selectivities determined from CBMC simulations at 300 K for all-silica FAU (Si/Al = ∞ with 192 Si, 0 Al, 0 Na^+ per unit

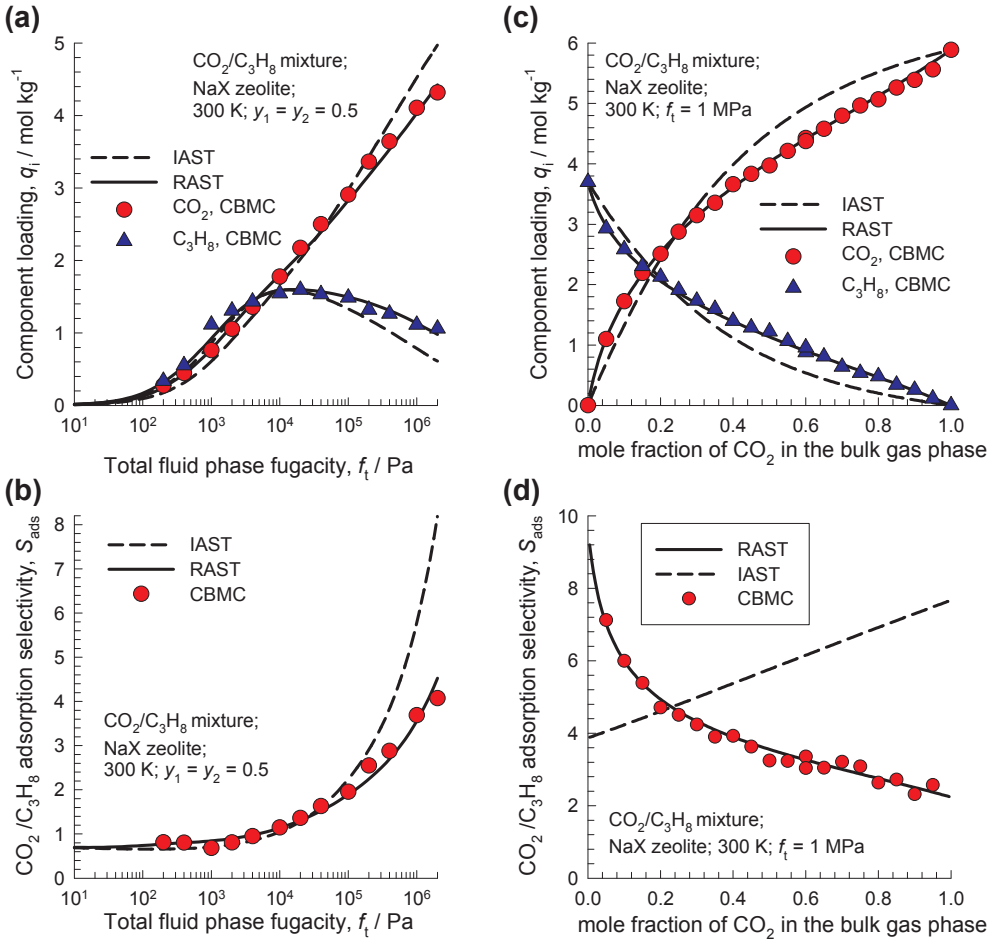

Fig. 2. (a, c) CBMC simulations (symbols) of the component loadings for $CO_2(1)/C_3H_8(2)$ mixture adsorption in NaX zeolite at 300 K. (b, d) CBMC simulations (symbols) of the $CO_2(1)/C_3H_8(2)$ adsorption selectivity. In (a, b), the *x*-axis is the total fugacity f_t in the bulk gas phase; the mole fraction of $CO_2(1)$ in the bulk gas phase is held constant, $y_1 = 0.5$. In (c, d), The IAST and RAST estimates are indicated by dashed and continuous solid lines, respectively. All data inputs and computational details are provided in the Supplementary Material.

cell), NaY (Si/Al = 2.56 with 138 Si, 54 Al, 54 Na^+ per unit cell), and NaX (Si/Al = 1.23 with 106 Si, 86 Al, 86 Na^+ per unit cell) zeolites with IAST estimations. For all-silica FAU, the IAST estimates are in perfect agreement with CBMC simulations. The agreement of IAST estimates with CBMC simulated data becomes progressively worse with decreasing Si/Al ratios. This trend confirms our contention that the failure of IAST is due to the strong interactions of CO_2 with extra-framework cations.

3. CBMC simulations of mixture adsorption in cation-exchanged LTA zeolite

We now investigate the accuracy of IAST estimates of $CO_2(1)/C_3H_8(2)$ mixture adsorption in LTA-4A zeolite, that consists of cages of 743 $Å^3$ volume, separated by 4.11 Å × 4.47 Å 8-ring windows. Per unit cell LTA-4A has 96 Si, 96 Al, 96 Na^+, with Si/Al = 1. In the CBMC simulations of $CO_2(1)/C_3H_8(2)$ mixture adsorption the mole fraction of $CO_2(1)$ in the bulk gas phase, y_1 was varied from 0 to 1, keeping the bulk gas phase mixture fugacity $f_t = f_1 + f_2$ constant at a value of 1 MPa; the results are summarized in Fig. 6a. The CBMC simulations show that the adsorption selectivity decreases with increasing proportion of $CO_2(1)$ in the bulk gas phase; see Fig. 6b. On the other hand, the IAST anticipates S_{ads} to be practically independent of y_1; this trend is similar to that witnessed in Fig. 1 e,f for the experimental data for $CO_2(1)/C_3H_8(2)$ mixture adsorption in ZSM-5 (Si/Al = 15), and H-MOR.

Fig. 7 shows computational snapshots of the location of $CO_2(1)$, and $C_3H_8(2)$ molecules within the pore topology of LTA-4A zeolite. We note that the CO_2 is almost exclusively located at the windows, or near the window entrance regions. Due to configurational restraints C_3H_8 can only located at the cage interiors. Consequently, the competition between the adsorption of CO_2 and C_3H_8 is less severe than assumed in the homogenous distribution that is inherent in the IAST prescription. The preferential perching of CO_2 at the window sites also manifests for other cage-window structures such as DDR, ERI, and CHA [23,37,38].

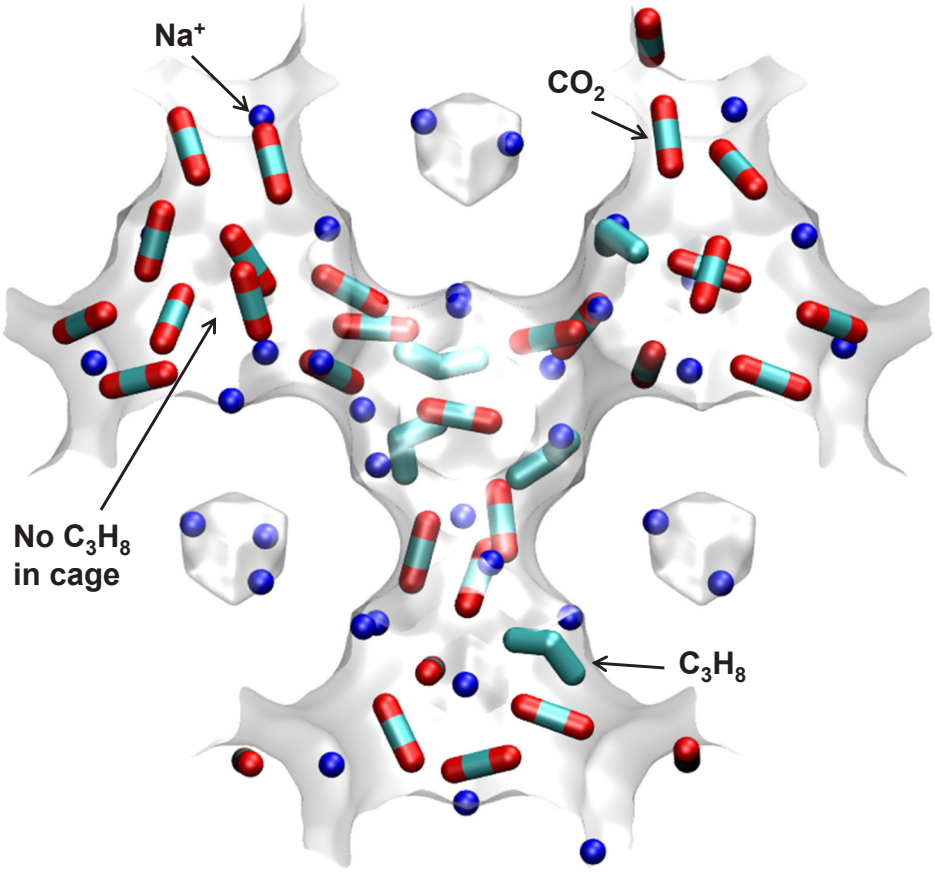

Fig. 3. Computational snapshots showing the location of CO_2, and C_3H_8 within the cages of NaX zeolite at 300 K and total fugacity f_t = 1 MPa. The component partial fugacities are f_1 = 0.45 MPa, and f_2 = 0.55 MPa.

4. Modelling non-ideal mixture adsorption using the RAST

For quantifying the departures of the IAST from CBMC data, we use the Real Adsorbed Solution Theory (RAST) [21,23,27–29,39], in which the partial fugacity of any component in the bulk fluid phase is related to the mole fraction x_i in the adsorbed phase by introduction of activity coefficients describing non-idealities in the adsorbed phase

$$f_i = P_i^0 x_i \gamma_i \tag{2}$$

From the CBMC data on $CO_2(1)/C_3H_8(2)$ mixture adsorption data in Fig. 2. the quantities $f_i/P_i^0 x_{i,CBMC}$ may be determined; these are plotted in Fig. 8a,b as function of (a) the mole fraction of CO_2 in the adsorbed phase, $x_{1,\mathrm{CBMC}}$, and (b) the adsorption potential, $\frac{\pi A}{RT}$. The plots show that appropriate models for the activity coefficient must also include the dependence on the adsorption potential [21,23,27–29,39]. The Wilson model, for example, may be written as

$$\begin{aligned}\ln(\gamma_1) &= \left(1-\ln(x_1 + x_2\Lambda_{12}) - \frac{x_1}{x_1 + x_2\Lambda_{12}} - \frac{x_2\Lambda_{21}}{x_2 + x_1\Lambda_{21}}\right)\left(1-\exp\left(-C\frac{\pi A}{RT}\right)\right)\\ \ln(\gamma_2) &= \left(1-\ln(x_2 + x_1\Lambda_{21}) - \frac{x_2}{x_2 + x_1\Lambda_{21}} - \frac{x_1\Lambda_{12}}{x_1 + x_2\Lambda_{12}}\right)\left(1-\exp\left(-C\frac{\pi A}{RT}\right)\right)\end{aligned} \tag{3}$$

In Eq. (3), C is a constant with the units kg mol^{-1}. The introduction of $\left(1-\exp\left(-C\frac{\pi A}{RT}\right)\right)$ imparts the correct limiting behaviors $\gamma_i \to 1$; $f_i \to 0$ for the activity coefficients in the Henry regime. As pore saturation conditions are approached, this correction factor tends to unity, $\left(1-\exp\left(-C\frac{\pi A}{RT}\right)\right) \to 1$. The total mixture loading is given by

$$q_t \equiv q_1 + q_2 = \frac{1}{\frac{x_1}{q_1^0(P_1^0)} + \frac{x_2}{q_2^0(P_2^0)} + [-x_1\ln(x_1 + x_2\Lambda_{12}) - x_2\ln(x_2 + x_1\Lambda_{21})]C\exp\left(-C\frac{\pi A}{RT}\right)} \tag{4}$$

The set of Eqs. (1), (2), (3), and (4) must be solved simultaneously to obtain the values of the component loadings q_1, and q_2, for a specified set of values of f_1, and f_2.

The continuous solid lines in Figs. 1, 2, and 6 represent RAST calculations in which the parameters in the Wilson model are obtained by fitting to match CBMC or experimental data on component loadings.

As illustration of the influence of thermodynamic non-idealities on the separation performance in fixed beds, let us consider CO_2/C_3H_8 separations in an adsorber packed with NaX zeolite operating at 300 K. Using the theory of shock waves for separations in fixed bed adsorbers [8,19], the maximum amount of pure C_3H_8 that can be recovered during the adsorption cycle is given by the separation potential, $\Delta Q = Q_{CO2}\frac{y_{C3H8}}{1-y_{C3H8}} - Q_{C3H8}$, expressed in the units mol per L of adsorbent; for these calculations the crystal framework density of NaX zeolite is taken as ρ = 1421 kg m^{-3}. Fig. 9. presents a comparison of the

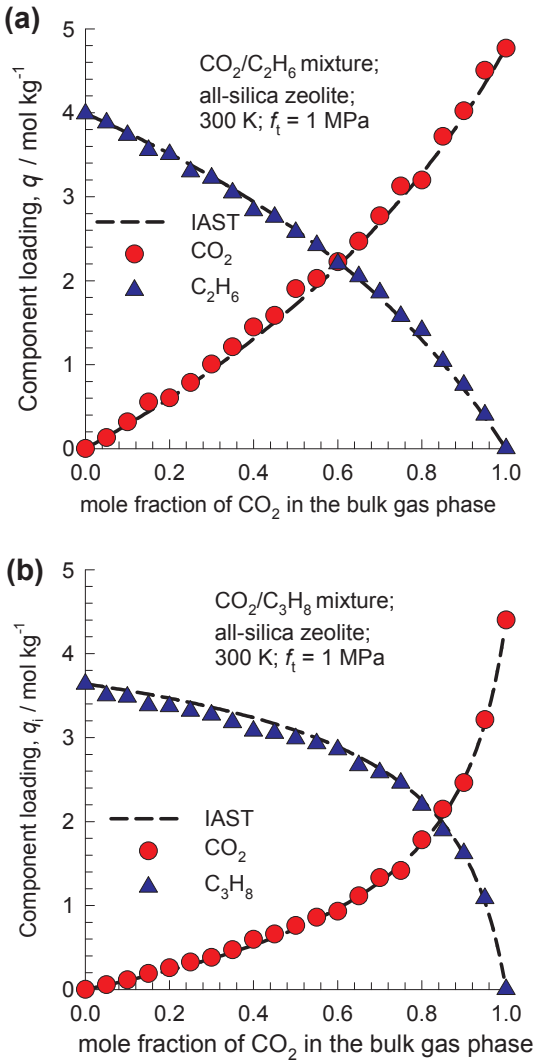

Fig. 4. CBMC simulations (symbols) of the component loadings for adsorption of (a) $CO_2(1)/C_3H_8(2)$, and (b) $CO_2(1)/C_2H_6(2)$ mixtures in all-silica FAU zeolite at 300 K and total fugacity f_t = 1 MPa. The x-axis represents the mole fraction of CO_2 in the bulk gas phase. The dashed line represent IAST estimates. All data inputs and computational details are provided in the Supplementary Material.

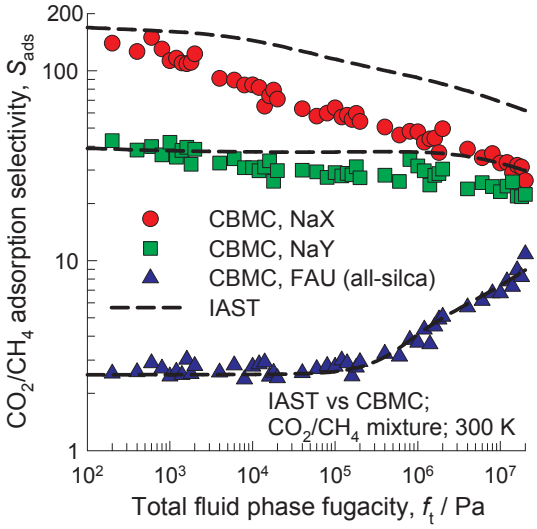

Fig. 5. Comparison CO_2/CH_4 adsorption selectivities determined from CBMC simulations 300 K for all-silica FAU (192 Si, 0 Al, 0 Na^+, Si/Al = ∞), NaY (138 Si, 54 Al, 54 Na^+, Si/Al = 2.56), and NaX (106 Si, 86 Al, 86 Na^+, Si/Al = 1.23) zeolites with IAST estimations. All data inputs and computational details are provided in the Supplementary Material.

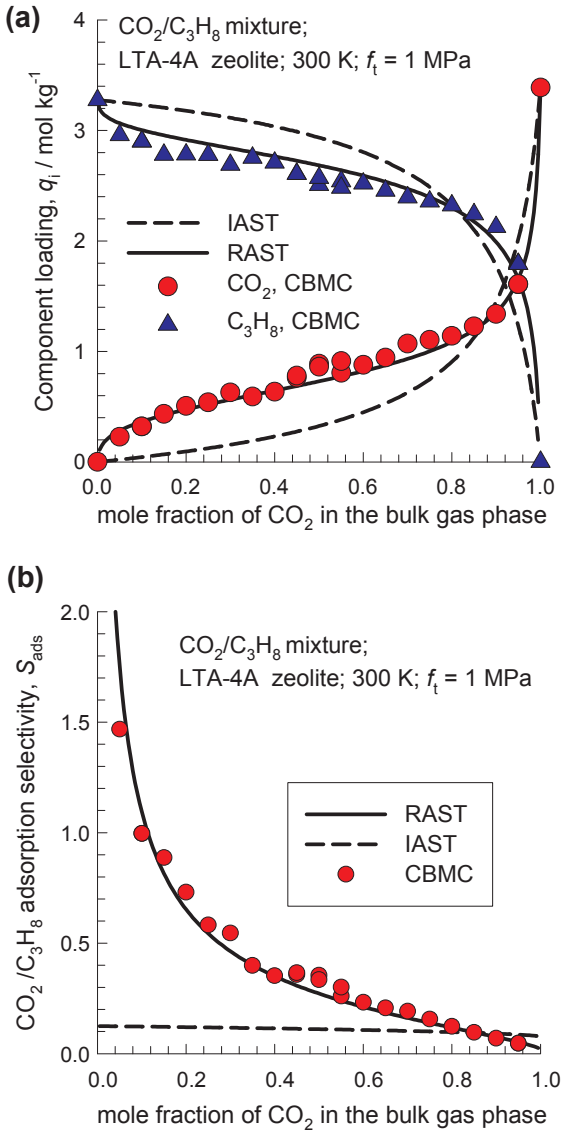

Fig. 6. (a) CBMC simulations (symbols) of the component loadings for $CO_2(1)/C_3H_8(2)$ mixture adsorption in LTA-4A zeolite at 300 K. The *x*-axis is mole fraction of CO_2 in the bulk gas phase; the total fugacity is held constant at $f_t = 1$ MPa. (b) CBMC simulations (symbols) of the $CO_2(1)/C_3H_8(2)$ adsorption selectivity. The IAST and RAST estimates are indicated by dashed and continuous solid lines, respectively. All data inputs and computational details are provided in the Supplementary Material.

IAST and RAST calculations of ΔQ; for a total mixture fugacity, $f_t = 1$ MPa, the values of ΔQ, are respectively 5.2, and 4 mol L^{-1}, respectively. Thermodynamic non-idealities reduce the productivity of pure C_3H_8 in a fixed bed adsorber by about 20%.

5. Conclusions

The following major conclusions emerge from the foregoing analysis of adsorption of CO_2-bearing mixtures in cation-exchanged zeolites. The failure of the IAST to provide quantitatively accurate estimates of mixture adsorption, as witnessed in the experimental data in Fig. 1. is ascribable to inhomogeneous distribution of adsorbates within the zeolite pores. In NaX zeolite, the inhomogeneity is a direct consequence of strong binding of CO_2 with extra-framework cations, leading congregation effects around cations. In LTA zeolites, CO_2 locates preferentially at the window regions, causing an inhomogeneous distribution of adsorbates. In the RAST description of mixture adsorption, the chosen model for activity coefficients must also include the dependence on the adsorption potential $\frac{\pi A}{RT}$.

The overall conclusion to be drawn from this study is that thermodynamic non-idealities may have a significant influence of the separations in fixed bed adsorption devices. For CO_2 capture applications with cation-exchanged zeolites, departures from idealities generally tend to reduce the separation effectiveness.

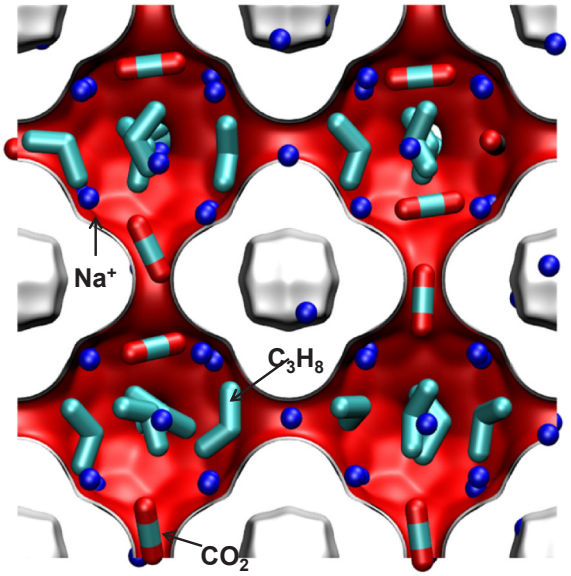

Fig. 7. Computational snapshots showing the location of CO_2, and C_3H_8 within the cages of LTA-4A zeolite at 300 K and total fugacity f_t = 1 MPa. The component partial fugacities are f_1 = 0.85 MPa, and f_2 = 0.15 MPa.

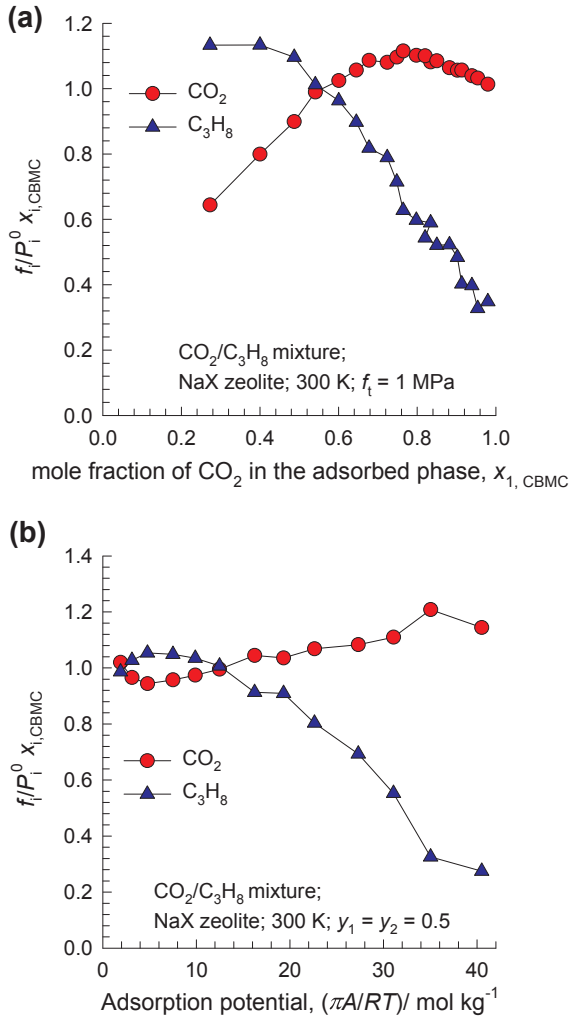

Fig. 8. Analysis of the non-idealities in $CO_2(1)/C_3H_8(2)$ mixture adsorption in NaX zeolite at 300 K. Dependence of $f_i/P_i^0 x_{i,CBMC}$ on (a) the mole fraction of CO_2 in the adsorbed phase as determined from CBMC simulations, $x_{1,CBMC}$, and (b) the adsorption potential, $\frac{\pi A}{RT}$. All data inputs and computational details are provided in the Supplementary Material.

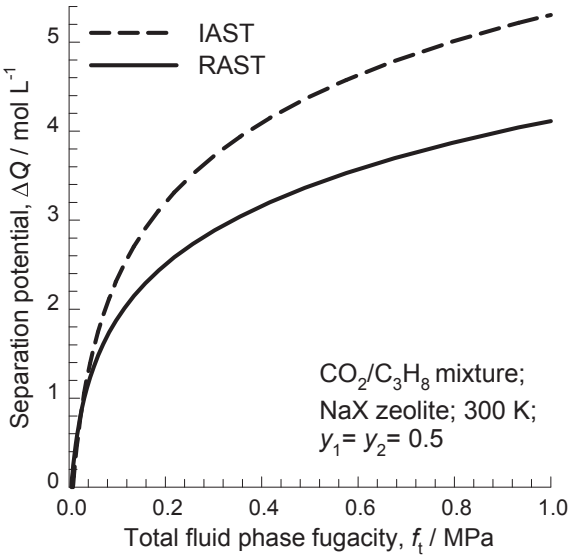

Fig. 9. Comparison of IAST and RAST calculations of the separation potential, $\Delta Q = Q_1 \frac{y_2}{y_1} - Q_2$ for separation of 50/50 $CO_2(1)/C_3H_8(2)$ feed mixtures in NaX zeolite at 300 K.

Appendix A. Supplementary material

Supplementary data associated with this article can be found, in the online version, at https://doi.org/10.1016/j.seppur.2018.06.009.

References

[1] G.D. Pirngruber, V. Carlier, D. Leinekugel-le-Cocq, Post-combustion CO_2 capture by vacuum swing adsorption using zeolites – a feasibility study, Oil Gas Sci. Technol. 69 (2014) 989–1003.

[2] J. Yang, R. Krishna, J. Li, J. Li, Experiments and simulations on separating a CO_2/CH_4 mixture using K-KFI at low and high pressures, Microporous Mesoporous Mater. 184 (2014) 21–27.

[3] M. Palomino, A. Corma, F. Rey, S. Valencia, New insights on CO_2 – methane separation using LTA zeolites with different Si/Al ratios and a first comparison with MOFs, Langmuir 26 (2010) 1910–1917.

[4] Y. Belmabkhout, G. Pirngruber, E. Jolimaitre, A. Methivier, A complete experimental approach for synthesis gas separation studies using static gravimetric and column breakthrough experiments, Adsorption 13 (2007) 341–349.

[5] R. Krishna, J.M. van Baten, In silico screening of zeolite membranes for CO_2 capture, J. Membr. Sci. 360 (2010) 323–333.

[6] R. Krishna, J.M. van Baten, In silico screening of metal-organic frameworks in separation applications, Phys. Chem. Chem. Phys. 13 (2011) 10593–10616.

[7] R. Krishna, J.M. van Baten, A comparison of the CO_2 capture characteristics of zeolites and metal-organic frameworks, Sep. Purif. Technol. 87 (2012) 120–126.

[8] R. Krishna, Methodologies for screening and selection of crystalline microporous materials in mixture separations, Sep. Purif. Technol. 194 (2018) 281–300.

[9] M.R. Hudson, L. Murray, J.A. Mason, D.W. Fickel, R.F. Lobo, W.L. Queen, C.M. Brown, Unconventional and highly selective CO_2 adsorption in zeolite SSZ-13, J. Am. Chem. Soc. 134 (2012) 1970–1973.

[10] F. Gholipour, M. Mofarahi, Adsorption equilibrium of methane and carbon dioxide on zeolite13X: experimental and thermodynamic modeling, J. Supercrit. Fluids 111 (2016) 47–54.

[11] M. Hefti, D. Marx, L. Joss, M. Mazzotti, Adsorption equilibrium of binary mixtures of carbon dioxide and nitrogen on zeolites ZSM-5 and 13X, Microporous Mesoporous Mater. 215 (2015) 215–228.

[12] M. Mofarahi, F. Gholipour, Gas adsorption separation of CO_2/CH_4 system using zeolite 5A, Microporous Mesoporous Mater. 200 (2014) 47–54.

[13] T.-H. Bae, M.R. Hudson, J.A. Mason, W.L. Queen, J.J. Dutton, K. Sumida, K.J. Micklash, S.S. Kaye, C.M. Brown, J.R. Long, Evaluation of cation-exchanged zeolite adsorbents for post-combustion carbon dioxide capture, Energy Environ. Sci. 6 (2013) 128–138.

[14] Y. Jiang, J. Ling, P. Xiao, Y. He, Q. Zhao, Z. Chu, Y. Liu, P. Li, P.A. Webley, Simultaneous biogas purification and CO_2 capture by vacuum swing adsorption using zeolite NaUSY, Chem. Eng. J. 334 (2018) 2593–2602.

[15] J. Bower, D. Barpaga, S. Prodinger, R. Krishna, H.T. Schaef, B.P. McGrail, M.A. Derewinski, R.K. Motkuri, Dynamic adsorption of CO_2/N_2 on cation-exchanged Chabazite SSZ-13: a breakthrough analysis, ACS Appl. Mater. Interfaces 10 (2018) 14287–14291.

[16] R.T. Yang, Adsorbents: Fundamentals and Applications, John Wiley & Sons Inc, Hoboken, New Jersey, 2003.

[17] J. Yang, H. Shang, R. Krishna, Y. Wang, K. Ouyang, J. Li, Adjusting the proportions of extra-framework K^+ and Cs^+ cations to construct a "molecular gate" on ZK-5 for CO_2 removal, Microporous Mesoporous Mater. 268 (2018) 50–57.

[18] D.M. Ruthven, S. Farooq, K.S. Knaebel, Pressure Swing Adsorption, VCH Publishers, New York, 1994.

[19] R. Krishna, Screening metal-organic frameworks for mixture separations in fixed-bed adsorbers using a combined selectivity/capacity metric, RSC Adv. 7 (2017) 35724–35737.

[20] R.T. Yang, Gas Separation by Adsorption Processes, Butterworth, Boston, 1987.

[21] A.L. Myers, J.M. Prausnitz, Thermodynamics of mixed gas, Adsorption 11 (A.I.Ch.E.J. 1965,) 121–130.

[22] R. Krishna, The Maxwell-Stefan description of mixture diffusion in nanoporous crystalline materials, Microporous Mesoporous Mater. 185 (2014) 30–50.

[23] R. Krishna, J.M. van Baten, R. Baur, Highlighting the origins and consequences of thermodynamic nonidealities in mixture separations using zeolites and metal-organic frameworks, Microporous Mesoporous Mater. 267 (2018) 274–292.

[24] J.A. Mason, K. Sumida, Z.R. Herm, R. Krishna, J.R. Long, Evaluating metal-organic frameworks for post-combustion carbon dioxide capture via temperature swing adsorption, Energy Environ. Sci. 4 (2011) 3030–3040.

[25] S. Divekar, A. Nanoti, S. Dasgupta, R. Aarti, P. Chauhan, M.O. Gupta, S.P. Garg, I.M. Mishra Singh, Adsorption equilibria of propylene and propane on zeolites and prediction of their binary adsorption with the ideal adsorbed solution theory, J. Chem. Eng. Data 61 (2016) 2629–2637.

[26] E. Mangano, D. Friedrich, S. Brandani, Robust algorithms for the solution of the ideal adsorbed, Solution Theory Eqs. 61 (A.I.Ch.E.J. 2015,) 981–991.

[27] F.R. Siperstein, A.L. Myers, Mixed-gas adsorption, AIChE J. 47 (2001) 1141–1159.

[28] O. Talu, A.L. Myers, Rigorous thermodynamic treatment of gas-adsorption, AIChE J. 34 (1988) 1887–1893.

[29] O. Talu, I. Zwiebel, Multicomponent adsorption equilibria of nonideal mixtures, AIChE J. 32 (1986) 1263–1276.

[30] C.-W. Wu, S. Sircar, Comments on binary and ternary gas adsorption selectivity, Sep. Purif. Technol. 170 (2016) 453–461.

[31] S.H. Hyun, R.P. Danner, Equiilbrium adsorption of ethane, ethylene, isobutane, carbon dioxide, and their binary mixtures on 13X molecular sieves, J. Chem. Eng. Data 27 (1982) 196–200.

[32] D. Frenkel, B. Smit, Understanding Molecular Simulations: From Algorithms to Applications, second ed., Academic Press, San Diego, 2002.

[33] B. Smit, R. Krishna, Molecular simulations in zeolitic process design, Chem. Eng. Sci. 58 (2003) 557–568.

[34] T.J.H. Vlugt, R. Krishna, B. Smit, Molecular simulations of adsorption isotherms for linear and branched alkanes and their mixtures in silicalite, J. Phys. Chem. B 103 (1999) 1102–1118.

[35] A. García-Sánchez, C.O. Ania, J.B. Parra, D. Dubbeldam, T.J.H. Vlugt, R. Krishna,

S. Calero, Development of a transferable force field for carbon dioxide adsorption in zeolites, J. Phys. Chem. C 113 (2009) 8814–8820.
[36] D. Dubbeldam, S. Calero, T.J.H. Vlugt, R. Krishna, T.L.M. Maesen, B. Smit, United atom forcefield for alkanes in nanoporous materials, J. Phys. Chem. B 108 (2004) 12301–12313.
[37] R. Krishna, J.M. van Baten, Segregation effects in adsorption of CO_2 containing mixtures and their consequences for separation selectivities in cage-type zeolites, Sep. Purif. Technol. 61 (2008) 414–423.
[38] R. Krishna, J.M. van Baten, Influence of segregated adsorption on mixture diffusion in DDR zeolite, Chem. Phys. Lett. 446 (2007) 344–349.
[39] J.J. Gutierrez-Sevillano, S. Calero, R. Krishna, Separation of benzene from mixtures with water, methanol, ethanol, and acetone: highlighting hydrogen bonding and molecular clustering influences in CuBTC, Phys. Chem. Chem. Phys. 17 (2015) 20114–20124.
[40] E. Costa, G. Calleja, A. Jimenez, J. Pau, Adsorption equilibrium of ethylene, propane, propylene, carbon dioxide, and their mixtures in 13X zeolite, J. Chem. Eng. Data 36 (1991) 218–224.
[41] G. Calleja, J. Pau, J.A. Calles, Pure and multicomponent adsorption equilibrium of carbon dioxide, ethylene, and propane on ZSM-5 zeolites with different Si/Al ratios, J. Chem. Eng. Data 43 (1998) 994–1003.